

Application of FAST Vision for Digital Terrain Model Generation

B.Kaiser, J.Hausladen, J.R.Tsay, B.P.Wrobel
Institute of Photogrammetry and Cartography
Technical University Darmstadt
Petersenstr.13
W-6100 Darmstadt
Federal Republic of Germany
Washington 1992 - Comm. IV

The construction of DTM together with its orthophoto based on pictures of a scale 1:12000 is carried out by facet stereo vision (=FAST Vision). It is regarded as a basic tool for a workstation of digital photogrammetry and a basic information source for geographic information systems. To evaluate a large surface, the DTM has to be generated stepwise with a scan-technique. Experiments are carried out with two different regularization methods - regularization by curvature minimization and adaptive regularization - and different regularization parameters. The image material used consisted of up to four aerial pictures of a rural area in Northern Germany and of pairs of computer generated pictures of simple geometric objects. The two regularization methods are compared and the advantage of using more than two pictures is investigated.

Keywords: DTM, image matching, orthophoto, rectification, 3-D

1. Introduction

The generation of DTMs and orthophotos plays an important part for geographic information systems. It can either be done by a human operator or by an automatic reconstruction process. Facets stereo vision (Wrobel, 1987) is such a method, which not only provides a digital terrain model and an orthophoto, but also statistical measures for the accuracy of the reconstruction. It works with object models for object surface and object grey values. Surface and orthophoto are approximated by finite elements, so-called facets. When a certain region of a surface (window) is reconstructed, it will be approximated by several Z-facets (height facets), which itself usually contain more than one G-facet (grey value facet). Radiometric differences between the digital images are modelled by a radiometric transfer function, which can be linear, constant or omitted at all. Details of the method are described in another paper at this congress (Wrobel et al., 1992b) and in (Weisensee, 1992; Wrobel et al., 1992a). The input data needed by FAST Vision are two or more digital images and the parameters of exterior and interior orientation.

The method results in an iterative process consisting of many steps, in which large systems of linear equations have to be solved. Each system of linear equations consists of hundreds of unknowns (the total number of unknowns is approximately the sum of the Z- and the G-facets). Therefore, it is impossible for reasons of computation time and computer memory to reconstruct a larger region of a surface without splitting this region into smaller windows for reconstruction. This results in a scan-technique for the reconstruction of larger areas (v. chapter 4). It was applied in the experiments with aerial pictures in this paper.

Surface reconstruction is an ill-posed problem (Wrobel et al., 1992a,b). Making additional qualitative assumptions to restrict the solution space yields a regularization method (Tikhonov, Arsenin, 1977). It is a very common approach to assume the reconstructed surface to be smooth. Thus, by adding a stabilizing functional expressing that assumption an ill-posed problem can be made well-posed. In the experiments in this paper two methods were applied: regularization by curvature minimization (a widely used approach) and by adaptive regularization (v. Wrobel et al. 1992a,b).

The experimental parameters are given in chapter 2. Chapter 3 explains the scan-technique used for the reconstruction of larger areas. Chapter 4 describes some computer-generated objects and images, being used for reconstruction experiments, and experimental results. In chapter 5 the same is done for aerial pictures of a rural area in Northern Germany. The experiments lead to some conclusions, which are drawn in chapter 6.

2. Parameters of Pictures and FAST Vision

a) Photogrammetric parameters

The aerial photographs were taken from a flying altitude of 1800m. The focal length was 153mm, the scale of the photographs is 1:12000. The pixel size in image space is $20\mu\text{m} \times 20\mu\text{m}$. The same photogrammetric data were used for the computer-simulated photographs of the generated objects.

b) FAST Vision parameters

The following parameters can be chosen for FAST Vision:

- size of the window to be reconstructed
- the break off criterion
- number of levels of the image pyramid
- size of the Z-facets
- number of G-facets per Z-facet
- the degree of the radiometric transfer function

With the exception of the first two ones and the latter one, the parameters chosen for the experiments of chapter 4 and chapter 5 were the same: The image pyramid consisted of 3 levels. Each Z-facet had a size of $2m \times 2m$ and contained 4×4 G-facets, which yielded approx. 2×2 pixels per G-facet. In the experiments with computer-generated images (chapter 4) the window used for reconstruction had a size of 12×12 Z-facets (= $24m \times 24m$ in object space = 48×48 G-facets). The difference of heights between two iterations was used as break-off criterion with $0.02m / 0.04m / 0.08m$ for interior grid heights, border heights and corner heights, respectively.

For the experiments with aerial pictures (chapter 5) windows with a different shape were used (v. chapter 3): Their size was 25×9 Z-facets (= $50m \times 18m = 100 \times 36$ G-facets). Break-off criterion: $0.10m / 0.20m / 0.40m$. In these experiments the differences concerning the grey values between the pictures were modelled by a linear radiometric transfer function. Such a function was not utilized in the experiments with computer-generated pictures, because there were no such differences to be modelled.

3. A Scan-Technique for the Reconstruction of larger areas

The number of variables of the system of normal equations set up by FAST Vision increases with the number of Z- and G-facets in the object window to be reconstructed and even more so does computation time for solving that system of equations. If the window contains $r \times s$ Z-facets and $p \times q$ G-facets, the total number of unknowns will amount to $(r+1) \times (s+1) + (p+1) \times (q+1)$. Thus, if the reconstruction of a larger surface with a fine resolution (i.e. small distances between the facets) is required, a scan-technique can be used. The window will be partitioned into smaller windows, which overlap each other. An especially efficient way of doing this is the use of so-called 'stripes', which are windows being very narrow in one direction. The application of a scan-technique using stripes results in a narrow band in the doubly bordered band diagonal coefficient matrix of the system of normal equations. In the experiments described in chapter 5 of this paper, stripes with 50% overlap were used.

4. Reconstruction with Computer-Generated Pictures

In order to be able to compare the results of reconstruction with the exact heights of a known object, which had to be reconstructed, several pairs of images were generated from various computer-generated surfaces (in the following denoted as original surfaces), which possessed certain geometric features. Four objects were generated:

- surface 1 (rf.par.=roof with a parallel ridge): a 'gable roof' consisting of two planes with an inclination of 20° meeting at a ridge, which is parallel to the X-coordinate axis and is the border between Z-facets. Thus curvature is 0 everywhere with the exception of the ridge. Fig. 4.9a shows an almost perfect reconstruction of this surface.
- surface 2 (rf.rot.=roof with rotated ridge): a 'gable roof' of the same shape, but the ridge forms an angle of 11.3° with the X-coordinate axis, see fig. 4.13a.
- surface 3 (cyl.par.=cylinder with parallel arc): a 'cylinder', which in fact is a surface generated by moving a parabola along a horizontal straight line. Curvature of this surface is 0 in direction of the X-axis of the object coordinate system. Fig. 4.6a gives an idea, how the original surface looks like.
- surface 4 (cyl.rot.=cylinder with rotated arc): another 'cylinder', looking like the before-mentioned surface, which is rotated in the X-Y-plane by 11.3° (see fig. 4.2a).

The grey values on the 'gable roof' ranged from 0 to 127 on the 'shady plane' of the roof and from 128 to 255 on the 'plane exposed to the sun'. Two computer-generated pictures of this surface can be seen in (Wrobel et al., 1992a,b). The texture on the 'cylinder' is very similar, but here the grey values range from 0 to 255.

Additionally to these grey values on the object surface there was an area of constant grey values (size: $8m \times 6m = 4 \times 3$ Z-facets) on some of the surfaces. This area is marked in the figures. It was introduced to study the behaviour of FAST Vision in areas, where grey values on the object surface do not contain any information, which can be used for surface reconstruction. It is especially interesting to see, how the two types of regularization - regularization by curvature minimization and adaptive regularization - are able to 'bridge' such areas of constant grey values. Otherwise, the matrix of normal equations set up by FAST Vision can become singular, if the objects contain such areas and no stabilizing functional is added (Wrobel et al., 1992a,b).

The computer-generated pictures of the above mentioned objects were taken with a standard deviation of 4 grey values (white noise). A pair of images was generated for each object.

As there are four surfaces and two types of texture on the surface of each object (with and without area of constant grey value), 8 pairs of images were generated. Of these, 7 were used for the reconstruction experiments. Surface 1 containing the area of constant grey values was not used, because similar experiments are shown in (Wrobel et al., 1992a,b). Multiplying these 7 data sets

with two types of regularization, the number of experiments amounts to 14. These and the respective figures were numbered as follows:

No. of experiment	type of surface	type of texture	type of regularization
1	surface 4 (cyl.rot.)	wcgv	adaptive
2	surface 4 (cyl.rot.)	wcgv	curv.min.
3	surface 4 (cyl.rot.)	ncgv	adaptive
4	surface 4 (cyl.rot.)	ncgv	curv.min.
5	surface 3 (cyl.par.)	ncgv	adaptive
6	surface 3 (cyl.par.)	ncgv	curv.min.
7	surface 3 (cyl.par.)	wcgv	adaptive
8	surface 3 (cyl.par.)	wcgv	curv.min.
9	surface 1 (rf.par.)	ncgv	adaptive
10	surface 1 (rf.par.)	ncgv	curv.min.
11	surface 2 (rf.rot.)	wcgv	adaptive
12	surface 2 (rf.rot.)	wcgv	curv.min.
13	surface 2 (rf.rot.)	ncgv	adaptive
14	surface 2 (rf.rot.)	ncgv	curv.min.

(wcgv = with constant grey value, ncgv = no constant grey value, adaptive = adaptive regularization, curv.min. = regularization by curvature minimization).

Table 4.1 shows some numerical results of these experiments, which were carried out using two different regularization parameters λ for each regularization method: $\lambda=2000$ and $\lambda=4000$. The shown values from the experiments are:

s_0 standard deviation of unit weight of the digital image grey values,

\bar{s}_z mean standard deviation of heights Z,

rms(dZ) root mean square of the differences between original surface and reconstructed surface,

dZmax maximum value of dZ,

dZmin minimum value of dZ.

dZmax and dZmin are the extreme values of the differences in the grid-points forming the grid of Z-facets with the exception of those grid-points situated on the borders of the window in object space, which was used for reconstruction.

$\lambda=2000$					
Exper. No.	s_0	\bar{s}_z metres	rms(dZ) metres	dZmax metres	dZmin metres
cyl.rot. = surface 4					
1	4.3	0.029	0.082	0.218	-0.322
2	4.3	0.029	0.041	0.074	-0.029
3	4.3	0.028	0.062	0.206	-0.145
4	4.4	0.028	0.040	0.075	-0.056
cyl.par. = surface 3					
5	3.9	0.025	0.089	0.133	-0.163
6	4.0	0.026	0.093	0.134	-0.127
7	3.9	0.026	0.092	0.131	-0.164
8	4.0	0.027	0.093	0.132	-0.124
rf.par. = surface 1					
9	3.9	0.033	0.063	0.121	-0.181
10	4.1	0.035	0.100	0.275	-0.176
rf.rot. = surface 2					
11	4.0	0.034	0.108	0.276	-0.411
12	4.2	0.035	0.114	0.472	-0.160
13	4.1	0.034	0.096	0.173	-0.390
14	4.3	0.035	0.092	0.251	-0.166

$\lambda=4000$					
Exper. No.	s_0	\bar{s}_z metres	rms(dZ) metres	dZmax metres	dZmin metres
cyl.rot. = surface 4					
1	4.3	0.024	0.062	0.148	-0.241
2	4.4	0.025	0.044	0.060	-0.036
3	4.3	0.023	0.051	0.147	-0.106
4	4.4	0.024	0.045	0.060	-0.044
cyl.par. = surface 3					
5	3.9	0.021	0.091	0.130	-0.177
6	4.0	0.022	0.099	0.133	-0.118
7	3.9	0.022	0.094	0.129	-0.183
8	4.0	0.023	0.099	0.134	-0.118
rf.par. = surface 1					
9	3.9	0.028	0.063	0.109	-0.207
10	4.2	0.030	0.128	0.349	-0.215
rf.rot. = surface 2					
11	4.0	0.028	0.099	0.287	-0.340
12	4.3	0.030	0.136	0.512	-0.220
13	4.1	0.028	0.087	0.136	-0.342
14	4.4	0.030	0.115	0.319	-0.219

Table 4.1 Numerical results of reconstruction experiments 1-14 with two different regularization parameters λ (For comparison: $\bar{s}_z = 0.18m$ corresponds to 0.1% of 'flying altitude')

Comparing the two regularization methods, it has to be noticed, that adaptive regularization yielded equal or lower standard deviations of unit weight and equal or lower standard errors of heights in all experiments. But which regularization method yields lower rms(dZ) depends very much on the surface to be reconstructed and on the regularization parameter λ chosen. As it had to be expected from theory and from the experiments in (Wrobel et al., 1992a,b), the ridge in surface 1 (rf.par.) is reconstructed best by adaptive regularization. The same is true for surface 3 (cyl.par.). In both cases the largest curvature of the original surface can be found at the borders between Z-facets and thus the smoothing effect of regularization by curvature minimization causes larger differences between original and reconstructed surface. However, it has to be said, that the advantage for adaptive regularization is only marginal, if surface 3 (cyl.par.) is reconstructed with reconstruction parameter $\lambda=2000$. With the same choice of λ , the reconstruction results of surface 2 (rf.rot.) are very similar for both regularization methods. If there is no area of constant grey value on the surface, the reconstructed surface is marginally closer to the original one when using regularization by curvature minimization. If surface 2 (rf.rot.) contains an area of constant grey value, the opposite is true. And the difference between original and reconstructed surface is clearly higher for adaptive regularization, when surface 4 (cyl.rot.) is reconstructed using $\lambda=2000$.

The choice of a higher regularization parameter $\lambda=4000$ shows, that regularization by curvature minimization is more sensitive to an increase in λ , if the surface contains edges: $rms(dZ)$ is distinctively lower for adaptive regularization in the case of reconstruction of the surfaces 1 (rf.par.) and 2 (rf.rot.). The reconstruction of the smooth surface 3 (cyl.par.) again yields only marginal differences in the $rms(dZ)$ -values for both regularization methods. The experiments 1-4 also show, that reconstruction with regularization by curvature minimization is closer to the original surface, if $\lambda=4000$ is chosen. But compared with $\lambda=2000$, the gap between the $rms(dZ)$ -values of both regularization methods has become closer.

In regularization by curvature minimization, the implied assumption of smoothness of a surface yields smooth reconstructed surfaces, which can be seen in fig. 4.2a, fig. 4.6a, fig. 4.8a, fig. 4.10a and fig. 4.12a (all surfaces reconstructed with $\lambda=2000$).

If the surface to be reconstructed itself is smooth, the reconstructed one shows great similarity to the original one. But if it is not, the surface edges will not be properly reconstructed, especially if a high regularization parameter λ is chosen.

All experiments show, that both regularization methods are capable of 'bridging' areas of low contrasts in image grey values.

Fig. 4.15 shows the standard deviation of heights for the reconstruction of surface 4 (cyl.rot.) containing an area of constant grey value, fig. 4.16 shows the standard deviation of heights for the reconstruction of the same surface, which does not contain such an area. Adaptive regularization was used in both cases. The distribution of standard errors looks very similar in both cases, with one exception: in the area of constant grey value the standard deviations of heights are higher in fig. 4.15 than those in the respective area in fig. 4.16. In that experiment the area to be 'bridged' is small, only 4×3 Z-facets. The increase of $\bar{\sigma}_Z$ is low, accordingly. But principally, these values can be used for the detection of regions of insufficient grey value information. Such areas could be marked in the reconstruction result, in order to inform a human operator of this situation.

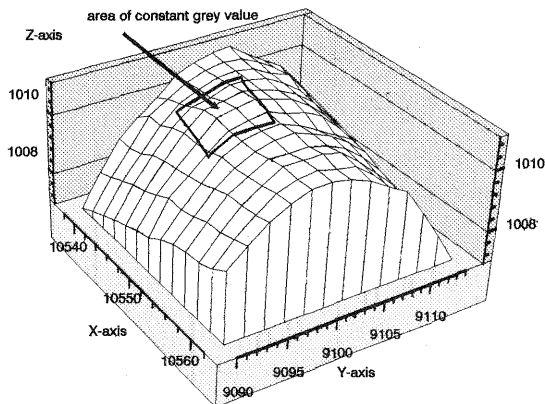


Fig. 4.1a Surface 4 with area of constant grey value: reconstructed surface FAST Vision with adaptive regularization

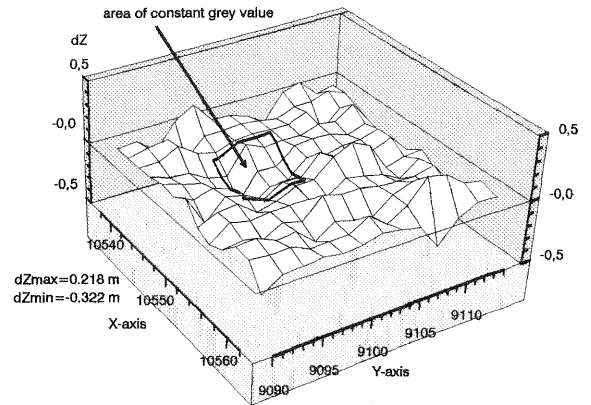


Fig. 4.1b Surface 4 with area of constant grey value: differences between original and reconstructed surface FAST Vision with adaptive regularization

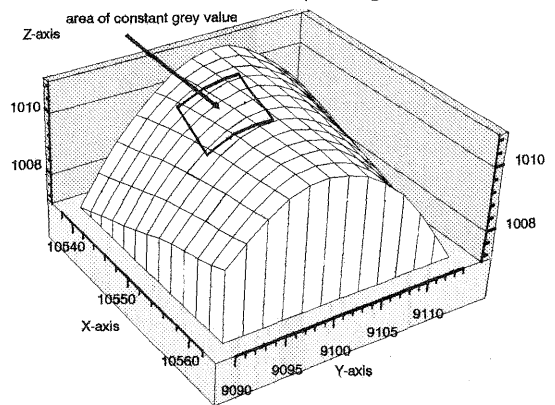


Fig. 4.2a Surface 4 with area of constant grey value: reconstructed surface FAST Vision with regularization by curvature minimization

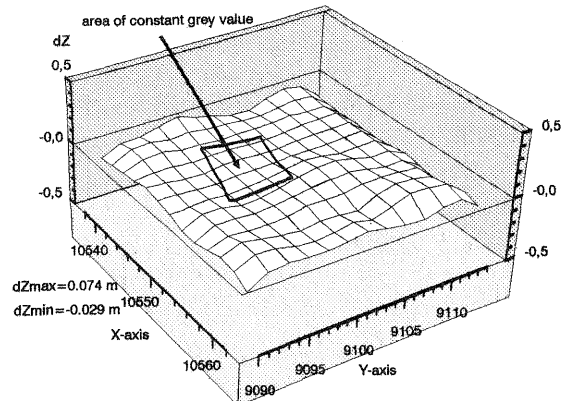


Fig. 4.2b Surface 4 with area of constant grey value: differences between original and reconstructed surface FAST Vision with regularization by curvature minimization

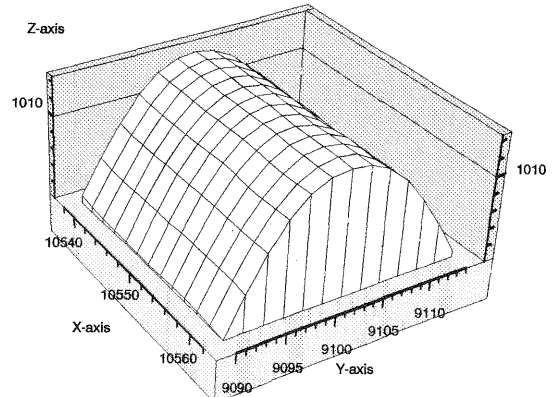


Fig. 4.6a Surface 3 without area of constant grey value: reconstructed surface FAST Vision with regularization by curvature minimization

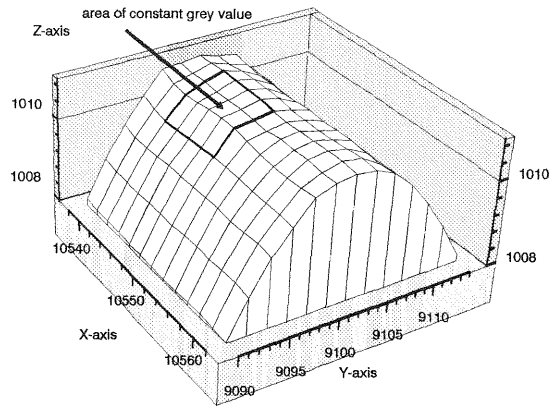


Fig. 4.7a Surface 3 with area of constant grey value:
reconstructed surface
FAST Vision with adaptive regularization

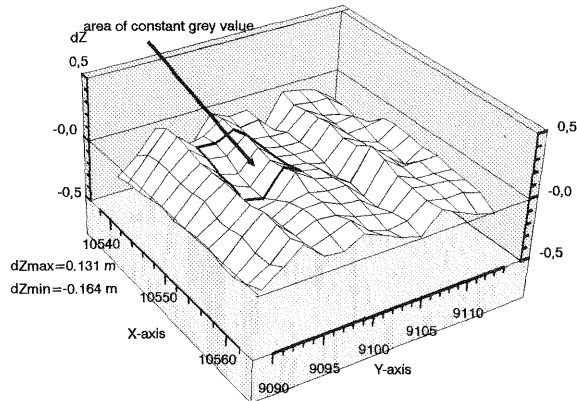


Fig. 4.7b Surface 3 with area of constant grey value:
differences between original and reconstructed surface
FAST Vision with adaptive regularization

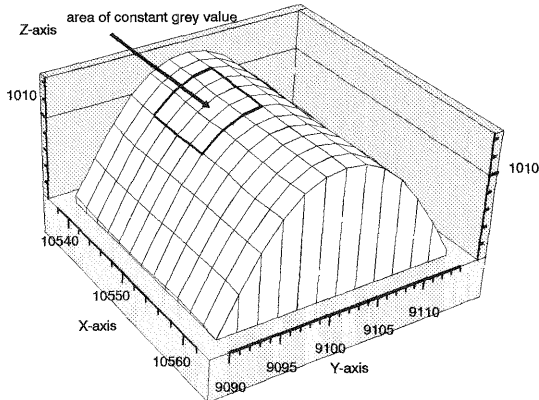


Fig. 4.8a Surface 3 with area of constant grey value:
reconstructed surface
FAST Vision with regularization by curvature minimization

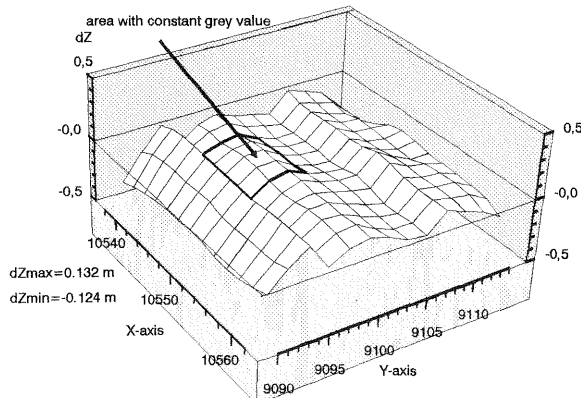


Fig. 4.8b Surface 3 with area of constant grey value:
differences between original and reconstructed surface
FAST Vision with regularization by curvature minimization

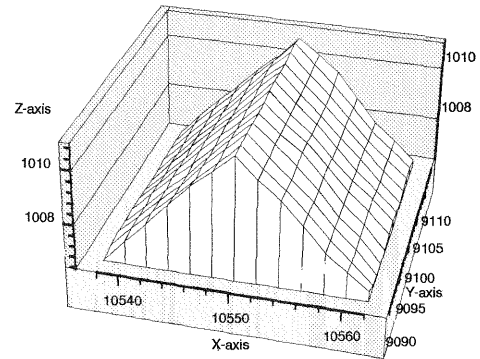


Fig. 4.9a Surface 1 without area of constant grey value:
reconstructed surface
FAST Vision with adaptive regularization

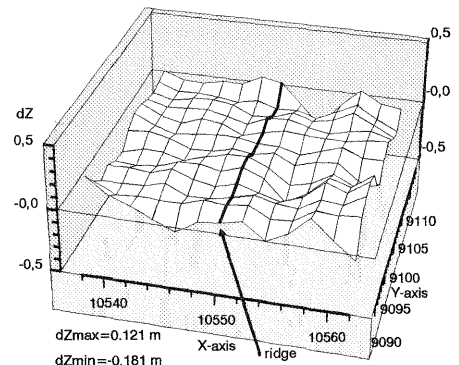


Fig. 4.9b Surface 1 without area of constant grey value:
differences between original and reconstructed surface
FAST Vision with adaptive regularization

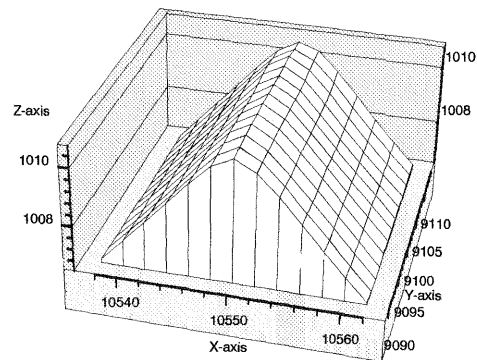


Fig. 4.10a Surface 1 without area of constant grey value:
reconstructed surface
FAST Vision with regularization by curvature minimization

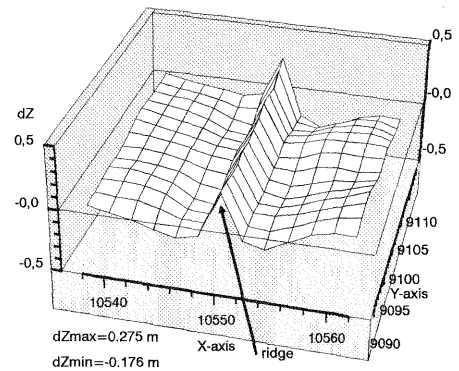


Fig. 4.10b Surface 1 without area of constant grey value:
differences between original and reconstructed surface
FAST Vision with regularization by curvature minimization

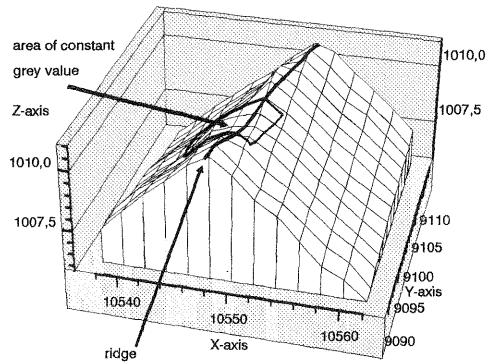


Fig. 4.11a Surface 2 with area of constant grey value: reconstructed surface FAST Vision with adaptive regularization

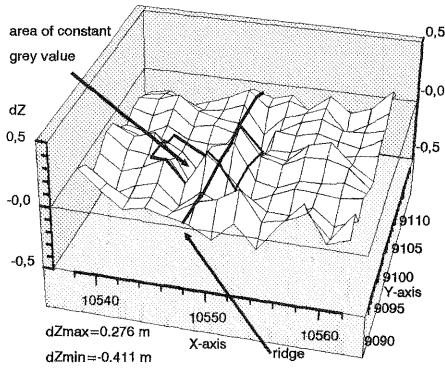


Fig. 4.11b Surface 2 with area of constant grey value: differences between original reconstructed surface FAST Vision with adaptive regularization

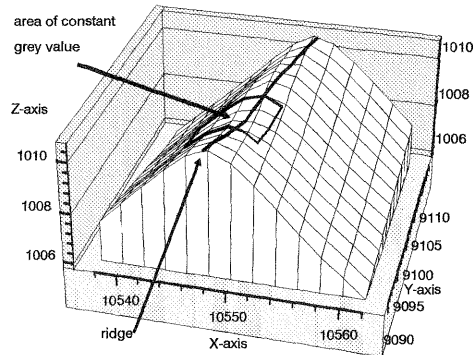


Fig. 4.12a Surface 1 with area of constant grey value: reconstructed surface FAST Vision with regularization by curvature minimization

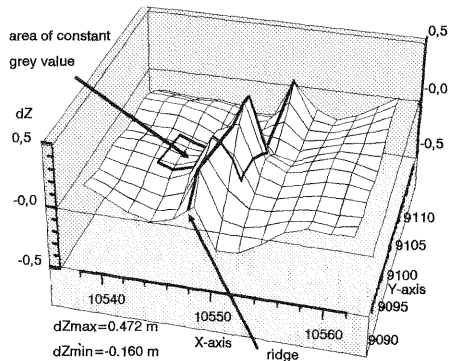


Fig. 4.12b Surface 1 with area of constant grey value: differences between original and reconstructed surface FAST Vision with regularization by curvature minimization

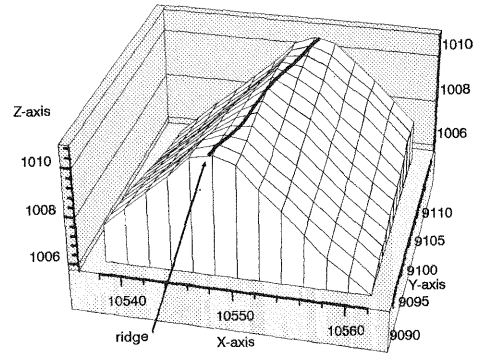


Fig. 4.13a Surface 1 without area of constant grey value: reconstructed surface FAST Vision with adaptive regularization

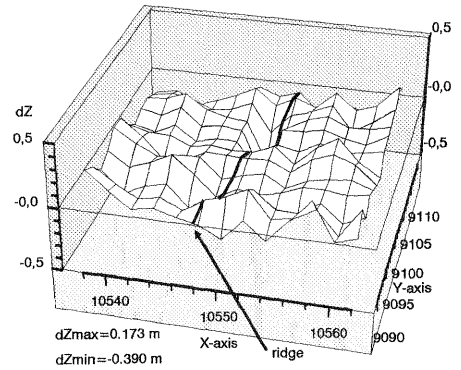


Fig. 4.13b Surface 1 without area of constant grey value: differences between original and reconstructed surface FAST Vision with adaptive regularization

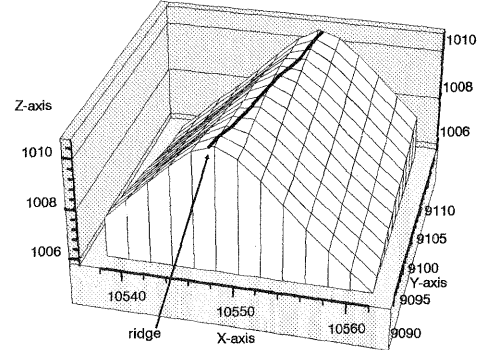


Fig. 4.14a Surface 1 without area of constant grey value: reconstructed surface FAST Vision with regularization by curvature minimization

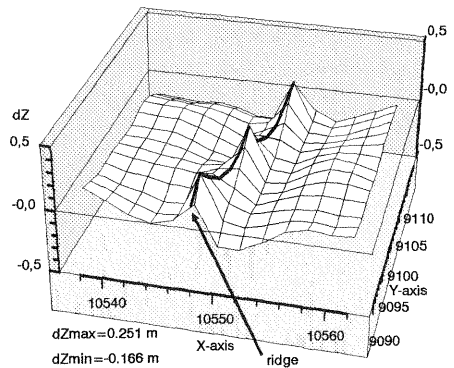


Fig. 4.14b Surface 1 without area of constant grey value: differences between original and reconstructed surface FAST Vision with regularization by curvature minimization

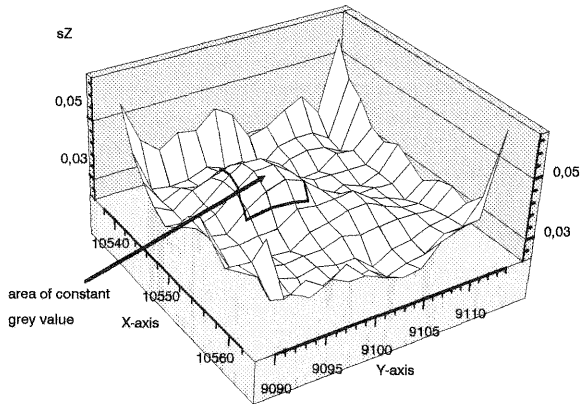


Fig. 4.15 Surface 4 with area of constant grey value: standard deviation of heights s_Z FAST Vision with adaptive regularization

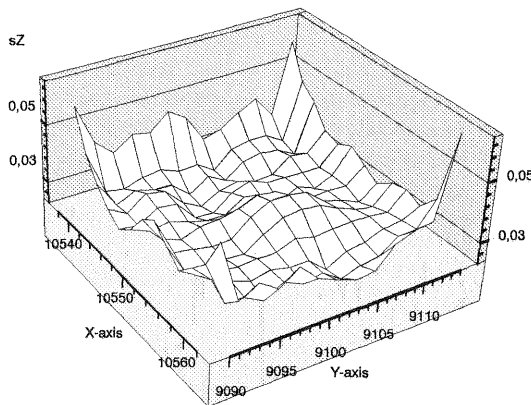


Fig. 4.16 Surface 4 without area of constant grey value: standard deviation of heights s_Z FAST Vision with adaptive regularization

5. Reconstruction with Aerial Pictures

One purpose of the experiments in this chapter is a comparison of the two regularization methods. The other is to study the different results of surface reconstruction using 2, 3 and 4 pictures. In order to achieve that, a set of aerial pictures with a longitudinal and lateral overlap of 60% was chosen. These were taken in a rural part of southeast Lower Saxony, a state in Northern Germany. The area to be reconstructed consists of fields and woods. The contrasts in the images are low. The scan-technique described in chapter 3 was used in order to limit the size of the systems of normal equations set up by FAST Vision. Table 5.1 shows the numerical results of the experiments, which were carried out with both regularization methods, with 2, 3 and 4 pictures and with regularization parameters $\lambda=2000$, $\lambda=4000$ and $\lambda=6000$. The area to be reconstructed was divided into 4 stripes of a size of 25×9 Z-facets. The numerical results for all experiments and all stripes are given in table 5.1. The values to be compared for different regularization methods, different regularization parameters and different numbers of pictures are:

- s_0 standard deviation of unit weight.
- \bar{s}_Z mean standard deviation of heights.

As in the experiments with computer-generated pictures, the standard deviations of unit weight were equal or lower, if adaptive regularization was used (only exception: stripe 4, $\lambda=6000$, 4 pictures). In general, the mean

standard deviation of heights also was equal or higher, if one chose regularization by curvature minimization (exceptions: stripe 3, $\lambda=4000$, 3 pictures ; stripe 3, $\lambda=6000$, 3 pictures ; stripes 3 and 4, $\lambda=6000$, 4 pictures). As the differences in these values were only marginal, the surface can be expected to have been smooth, so that the assumption of smoothness implied in regularization by curvature minimization is true. Standard deviation of unit weight and mean standard deviations slightly increase with increasing regularization parameter λ , which shows, that λ should be chosen as low as possible in order to get good reconstruction result. But on the other hand it has to be chosen high enough to guarantee, that the break-off criterion is met. As the difference in the numerical results does not depend very much on the choice of λ , this choice is not a crucial point, which again indicates, that the surface is smooth.

n_p	λ	St. no.	regularization					
			curvat. min.			adaptive		
			s_0	\bar{s}_Z	n_i	s_0	s_Z	n_i
2	2000	1	6.6	0.065	4	6.3	0.062	17
2	2000	2	7.0	0.051	4	6.6	0.049	10
2	2000	3	7.8	0.064	12	7.6	0.062	11
2	2000	4	8.4	0.074	12	8.1	0.070	50
2	4000	1	6.7	0.055	4	6.5	0.053	6
2	4000	2	7.0	0.043	4	6.7	0.041	6
2	4000	3	7.9	0.054	12	7.6	0.052	16
2	4000	4	8.5	0.063	12	8.3	0.061	20
2	6000	1	6.7	0.050	4	6.5	0.048	6
2	6000	2	7.0	0.038	4	6.8	0.037	6
2	6000	3	7.9	0.049	12	7.6	0.047	16
2	6000	4	8.5	0.056	12	8.3	0.055	20
3	2000	1	4.3	0.045	3	4.2	0.045	5
3	2000	2	4.5	0.035	3	4.4	0.035	7
3	2000	3	5.1	0.044	4	5.1	0.043	50
3	2000	4	5.6	0.052	3	5.5	0.049	50
3	4000	1	4.3	0.038	3	4.3	0.038	4
3	4000	2	4.6	0.029	3	4.5	0.029	6
3	4000	3	5.2	0.037	4	5.1	0.038	7
3	4000	4	5.6	0.043	3	5.5	0.041	50
3	6000	1	4.3	0.034	3	4.2	0.033	4
3	6000	2	4.6	0.026	3	4.5	0.026	4
3	6000	3	5.2	0.033	3	5.1	0.034	5
3	6000	4	5.6	0.039	3	5.6	0.037	50
4	2000	1	4.0	0.042	3	4.0	0.041	5
4	2000	2	4.4	0.034	3	4.2	0.033	7
4	2000	3	5.0	0.043	4	5.0	0.043	3
4	2000	4	5.4	0.049	3	5.3	0.048	44
4	4000	1	4.0	0.035	3	4.0	0.035	3
4	4000	2	4.5	0.028	7	4.3	0.027	6
4	4000	3	5.0	0.036	3	5.0	0.036	7
4	4000	4	5.4	0.041	14	5.2	0.041	50
4	6000	1	4.0	0.032	3	4.0	0.032	3
4	6000	2	4.5	0.026	3	4.3	0.024	6
4	6000	3	5.0	0.032	3	5.0	0.033	5
4	6000	4	5.4	0.037	13	5.5	0.040	3

Table 5.1 Numerical results of surface reconstruction with 2, 3 and 4 aerial pictures (n_p =number of pictures, n_i =number of iterations, $n_i=50 \Rightarrow$ convergence criterion was not met in 50 iterations, St.no. = No. of stripe)

The greatest difference in the values of s_0 and \bar{s}_Z occurs, if different numbers of pictures are used for surface reconstruction with FAST Vision. The values are the lower, the more pictures are used. Fig. 5.1 shows s_0 for all stripes and all numbers of pictures for regularization by curvature minimization and $\lambda=2000$. Fig. 5.2 shows \bar{s}_Z for the same case.

The number of iterations using adaptive regularization is almost always higher than that using regularization by curvature minimization. This effect results from the higher degree of freedom of adaptive regularization.

A comparison of the heights resulting from automatic surface reconstruction with FAST Vision and the values measured by a human operator will be carried out in the near future.

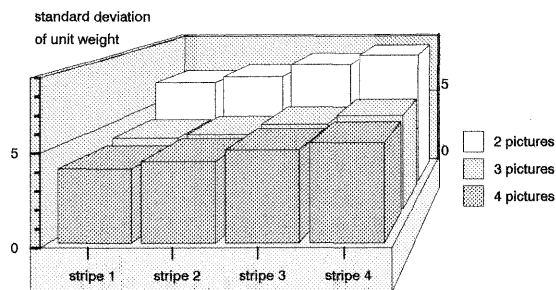


Fig. 5.1: Standard deviation of unit weight dependent on number of pictures used for FAST Vision

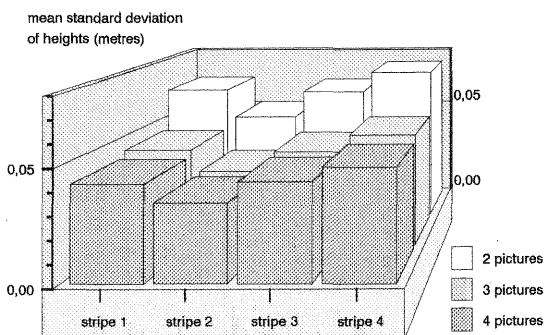


Fig. 5.2: Mean standard deviation of heights dependent on number of pictures used for FAST Vision

6. Conclusions

Two aspects were important in the experiments carried out in this paper: How will the results of the reconstruction of different surfaces differ, if both methods of regularization, regularization by curvature minimization or by adaptive regularization, are used? And will there be a noticeable improvement in the reconstruction of surfaces, if the input data consists of more than two pictures?

The answer to the latter question is clearly positive. The addition of a third picture not only lowers the values of standard deviation of unit weight and the mean standard deviations of heights, but also cuts down the number of iterations necessary to meet the break-off criterion. Using four instead of three pictures does not result in such a big improvement, but one has to keep in mind, that one of three pictures or its orientation data might be of poorer quality. Then, the addition of a fourth picture would increase the reliability of the reconstruction results.

The comparison of the two regularization methods depends on several parameters. Surfaces containing edges are better reconstructed using adaptive regularization, whereas the assumption of smoothness implied in regularization by curvature minimization yields better reconstruction of smooth surfaces as long as the regularization parameter λ is chosen not too high. Surface 1 (rf.par.) and 2 (rf.rot.) are composed of Z-facets with zero curvature almost everywhere. On surfaces 3 (cyl.par.) and 4 (cyl.rot.) one of the principal curvatures is zero everywhere and the other varies from almost zero to low values only. So, there are good conditions for applying regularization by curvature minimization. The second method - adaptive regularization - is practically independent of the type of surface curvatures, but as it offers much more degrees of freedom to the object surface model the results show up more roughness than with the first method. Adaptive regularization was introduced in order to yield reconstruction results not so dependent on that choice of λ , this property is confirmed by the experiments: The reconstruction results derived from regularization by curvature minimization get worse with increasing λ in general, which is not true if adaptive regularization is used. The price to be paid for using adaptive regularization is a higher number of iterations.

7. References

- Tikhonov, A.N./Arsenin, V.Y.: Solutions of Ill-Posed Problems. V.H. Winston & Sons, Washington D.C., 1977
- Weisensee, M.: Modelle und Algorithmen für das Facetten-Stereosehen. Deutsche Geodätische Kommission, Reihe C, Nr. 374, München, 1992
- Wrobel, B.: Digital Image Matching by Facets Using Object Space Models. 4th International Symposium on Optical and Optoelectr. Appl. Science and Engineering, March 30th-April 3rd 1987, The Hague, Netherlands, SPIE 804, p.p. 325-333
- Wrobel, B.: The Evolution Of Digital Photogrammetry From Analytical Photogrammetry. Photogrammetric Record, 13(77), p.p. 765-776, April 1991
- Wrobel, B./Kaiser, B./Hausladen, J.: Adaptive Regularization of Surface Reconstruction By Image Inversion. In: Förstner, W./Ruwiedel, St. (eds) : Robust Computer Vision. Wichmann Verlag, Karlsruhe 1992, (Wrobel et al., 1992a)
- Wrobel, B./Kaiser, B./Hausladen, J.: Adaptive Regularization - a New Method for Stabilization of Surface Reconstruction from Images. Presented Paper, XVIIth Congress of ISPRS, Comm. III/2, Washington 1992, (Wrobel et al., 1992b)

These investigations are supported by Deutsche Forschungsgemeinschaft.